Journal of Zhejiang University-SCIENCE B (Biomedicine & Biotechnology) 2025 26(1):76-91
www.jzus.zju.edu.cn; www.springer.com/journal/11585
E-mail: jzus_b@zju.edu.cn

Research Article

https://doi.org/10.1631/jzus.B2300896

Chronic exposure to hexavalent chromium induces esophageal tumorigenesis via activating the Notch signaling pathway

Yilin ZHU[1], Fanrong LIU[1], Lei LIU[1], Jinfu WANG[1], Fengyuan GAO[1], Lan YE[2], Honglei WU[3], Chengjun ZHOU[4], Guimei LIN[5,6], Xiaogang ZHAO[1,7], Peichao LI[1,7]✉

[1]*Department of Thoracic Surgery, The Second Hospital, Cheeloo College of Medicine, Shandong University, Jinan 250012, China*
[2]*Cancer Center, The Second Hospital, Cheeloo College of Medicine, Shandong University, Jinan 250012, China*
[3]*Department of Gastroenterology, The Second Hospital, Cheeloo College of Medicine, Shandong University, Jinan 250012, China*
[4]*Department of Pathology, The Second Hospital, Cheeloo College of Medicine, Shandong University, Jinan 250012, China*
[5]*Key Laboratory of Chemical Biology (Ministry of Education), School of Pharmaceutical Sciences, Cheeloo College of Medicine, Shandong University, Jinan 250012, China*
[6]*National Medical Products Administration Key Laboratory for Technology Research and Evaluation of Drug Products, Shandong University, Jinan 250012, China*
[7]*Key Laboratory of Chest Cancer, The Second Hospital, Cheeloo College of Medicine, Shandong University, Jinan 250012, China*

Abstract: Hexavalent chromium Cr(VI), as a well-established carcinogen, contributes to tumorigenesis for many human cancers, especially respiratory and digestive tumors. However, the potential function and relevant mechanism of Cr(VI) on the initiation of esophageal carcinogenesis are largely unknown. Here, immortalized human esophageal epithelial cells (HEECs) were induced to be malignantly transformed cells, termed HEEC-Cr(VI) cells, via chronic exposure to Cr(VI), which simulates the progress of esophageal tumorigenesis. In vitro and in vivo experiments demonstrated that HEEC-Cr(VI) cells obtain the ability of anchorage-independent growth, greater proliferative capacity, cancer stem cell properties, and the capacity to form subcutaneous xenografts in BALB/c nude mice when compared to their parental cells, HEECs. Additionally, HEEC-Cr(VI) cells exhibited weakened cell motility and enhanced cell adhesion. Interestingly, HEECs with acute exposure to Cr(VI) failed to display those malignant phenotypes of HEEC-Cr(VI) cells, suggesting that Cr(VI)-induced malignant transformation, but not Cr(VI) itself, is the cause for the tumor characteristics of HEEC-Cr(VI) cells. Mechanistically, chronic exposure to Cr(VI) induced abnormal activation of Notch signaling, which is crucial to maintaining the capacity for malignant proliferation and stemness of HEEC-Cr(VI) cells. As expected, *N*-[*N*-(3,5-difluorophenacetyl)-L-alanyl]-*S*-phenylglycine *t*-butyl ester (DAPT), an inhibitor for the Notch pathway, drastically attenuated cancerous phenotypes of HEEC-Cr(VI) cells. In conclusion, our study clarified the molecular mechanism underlying Cr(VI)-induced esophageal tumorigenesis, which provides novel insights for further basic research and clinical therapeutic strategies about Cr(VI)-associated esophageal cancer.

Key words: Hexavalent chromium Cr(VI); Esophageal tumorigenesis; Malignant proliferation; Stemness; Notch signaling pathway

1 Introduction

Esophageal cancer (EC) ranks 7th and 6th in the incidence of human malignant tumors and cancer-related causes of death, respectively, which has been a huge threat to human health (Sung et al., 2021). Esophageal squamous cell carcinoma (ESCC) and esophageal adenocarcinoma (EAC) are two main pathological subtypes that show great variances in their biological characteristics and geographical distribution (Abnet et al., 2018; Morgan et al., 2022). Although current therapy for EC involves chemoradiotherapy, esophagectomy, targeted therapy, and emerging immunotherapies, five-year survival rates of EC patients are approximately 12%–20% (An et al., 2023). Among all factors contributing to EC tumorigenesis, environmental pollutants, especially carcinogenic metal ions, attracted more and more research attention (Lee

✉ Peichao LI, lipeichao@email.sdu.edu.cn
Peichao LI, https://orcid.org/0009-0003-0126-602X
Yilin ZHU, https://orcid.org/0009-0000-5100-5547

Received Dec. 10, 2023; Revision accepted June 17, 2024;
Crosschecked Sept. 9, 2024; Published online Oct. 21, 2024

et al., 2016; Jiang et al., 2021; Nozadi et al., 2021; Sohrabi et al., 2021).

Hexavalent chromium Cr(VI), a well-established carcinogenic metal, is widely distributed in human living environments due to its extensive applications in industrial processes such as plating, stainless steel manufacturing, dyes and pigments, and leather tanning (Iyer et al., 2023). Humans are exposed to Cr(VI) contamination mainly through inhalation, drinking water, and food (Sun et al., 2015). Once entering cells, Cr(VI) is reduced to trivalent Cr(III) by glutathione, whereby the production of reactive oxygen species (ROS), formation of Cr-DNA adducts, damage and mutagenesis of the genome, and mitochondrial dysfunction are considered dominant molecular mechanisms underlying Cr(VI) toxicity (Chen et al., 2019). Cr(VI)-induced tumorigenesis has been reported in some murine models and human cells (Islam et al., 2022). For instance, a two-year study from the National Toxicology Program revealed that chronic oral exposure to Cr(VI) (180 mg/L) through drinking water induced the experimental rats and mice to develop cancer in the oral cavity and the small intestine, respectively (National Toxicology Program, 2008; Stout et al., 2009). Male A/J mice with inhalation exposure to Cr(VI) developed bronchioloalveolar adenomas and carcinomas in their lungs (Zeidler-Erdely et al., 2020). After long-term exposure (for 20 weeks) to Cr(VI), female C57BL/6J mice formed colorectal cancer and displayed a significant upregulation of proliferative cell nuclear antigen (PCNA) (Zhang et al., 2020). So far, studies exploring the effects of Cr(VI) exposure on human cells have mainly focused on human bronchial epithelial cells (16-HBE and BEAS-2B). For example, studies by Hu et al. (2016, 2018) revealed that Cr(VI) exposure induced hypermethylation of cyclin-dependent kinase inhibitor 2A (*CDKN2A*), tumor protein P53 (*TP53*), and DNA repair genes in 16-HBE cells. Sun et al. (2011) and Li PC et al. (2021) reported that Cr(VI) exposure-mediated downregulation of hedgehog-interacting protein (HHIP) significantly induced the malignant transformation of BEAS-2B cells. However, the association between Cr(VI) and esophageal tumorigenesis and its potential molecular mechanisms have not been fully explored.

Notch signaling, as an evolutionarily conserved pathway, deeply participates in the regulation of development, homeostasis, and renewal in multiple tissues and organs (Zhou et al., 2022). When ligand-mediated activation occurs, Notch receptors are cleaved three times to be the active truncation. Then, the truncated Notch protein is translocated into the nucleus to regulate the transcription of downstream target genes (Kopan and Ilagan, 2009). Attributed to the crucial and pleiotropic physiological roles of the Notch pathway, its dysregulation has been reported to be closely associated with the initiation, progression, immunotherapy, and clinical prognoses in various human cancers (Li et al., 2023; Cai et al., 2024). It is worth noting that the activity status and potential function of the Notch signaling pathway in esophageal epithelial cells with chronic exposure to Cr(VI) remain largely unknown.

In the present study, immortalized human esophageal epithelial cells (HEECs) were applied for long-term exposure to Cr(VI), which simulates the progress of esophageal tumorigenesis. In vitro and in vivo experiments were used to evaluate the malignant proliferation of the transformed cell line, named HEEC-Cr(VI). Mechanistically, we revealed aberrant activation of the Notch signaling in HEEC-Cr(VI) cells based on RNA sequencing data. Furthermore, we assessed the ability to proliferate malignantly in HEEC-Cr(VI) cells treated with an inhibitor for the Notch pathway. Our results illuminate the molecular mechanism underlying the initiation of EC induced by Cr(VI), which provides important evidence and promising insights for further studies and treatment strategies about Cr(VI)-associated EC.

2 Materials and methods

2.1 Cell culture

HEECs, also known as HEsEpiCs, were isolated from the human esophagus in the ScienCell Research Laboratories (Carlsbad, CA, USA). Detailed information about HEECs can be found on the website (https://sciencellonline.com/human-esophageal-epithelial-cells). HEECs were purchased from the BeNa Culture Collection (Beijing, China) and authenticated by Short Tandem Repeat analysis with Tsingke Biotechnology (Beijing, China). The Dulbecco's modified Eagle's medium (DMEM) (10-013-CVRC; Corning, Shanghai, China) supplemented with 1% (volume fraction) penicillin/streptomycin (PS) (C125C5; NCM Biotech, Jiangsu, China) and 10% (volume fraction) fetal bovine serum (FBS) (FSP500; ExCell Bio, Jiangsu,

China) was applied for cell culturing. All cells were grown in an incubator with 5% CO_2 at 37 ℃.

2.2 Establishment of transformed cells induced by Cr(VI)

HEECs were cultured in the complete medium (DMEM supplemented with 10% FBS and 1% PS) containing 0.25 or 0.50 μmol/L of Cr(VI). When the confluence of cultured cells was approximately 90%, the cell passaging was performed. It should be noted that the limited expansion capacity of HEECs restricts their long-term cultures according to the information from the ScienCell Research Laboratories. The potassium chromate (K_2CrO_4) (216615; Sigma-Aldrich, Shanghai, China) was applied for Cr(VI) exposure. Interestingly, HEECs with ongoing exposure to Cr(VI) (0.25 μmol/L) displayed an increasingly strong capability for amplification. However, after a few weeks of exposure to Cr(VI) (0.50 μmol/L), HEECs failed to maintain enough viability for the passaging. Every ten generations, the soft agar colony formation assay was applied to evaluate the anchorage-independent growth of HEECs with chronic Cr(VI) exposure. Finally, after 60 generations of exposure to Cr(VI) (0.25 μmol/L), the transformed HEEC cell line possessed the significant capacity to anchorage-independently grow in the soft agar and was named HEEC-Cr(VI).

2.3 Mice and xenograft models

BALB/c athymic nude mice (four weeks old; male) were obtained from Beijing Vital River Laboratory Animal Technology Co., Ltd. (Beijing, China). Mice were housed in a ventilated cage with a 12-h light/dark cycle, a temperature between 18 ℃ and 23 ℃, and 40%–60% relative humidity. To establish xenograft models, each nude mouse was subcutaneously injected with 5×10^6 cells in the axillary fossa. Tumor sizes were measured every 4 d and calculated with the following formula: (longest-diameter×shortest-diameter^2)/2. The mice were euthanized when the maximum volume of xenografts reached or exceeded 1000 mm^3.

2.4 Soft agar colony formation assay

Cells were suspended in culture medium supplemented with 1% PS, 10% FBS, and 0.35% (3.5 g/L) low-melting-point agarose (A4018; Sigma-Aldrich) and were then added into six-well plates with medium containing 0.50% low-melting-point agarose on the bottom for three weeks. Detailed procedures and the counting method were described in our previous study (Li PC et al., 2021).

2.5 EdU incorporation assay

A total of 5×10^3 cells were cultured into each well of a 96-well plate for 24 h. The BeyoClick™ EdU-594 Kit (C0078S; Beyotime Biotechnology, Shanghai, China) was applied for the assay. After the culture medium was discarded, 100 μL of 5-ethynyl-2-deoxyuridine (EdU) solution was added into each well for 2 h of incubation. Then, 4% (volume fraction) paraformaldehyde was utilized to fix the cells. After being washed with 3% (volume fraction) bovine serum albumin (BSA) and permeabilized by 0.3% (volume fraction) Triton X-100, the cells were incubated with click reaction buffer for 30 min followed by nuclear staining with Hoechst 33342 solution (AG51012; Accurate Biology, Hunan, China). Images were captured using a fluorescence microscope. The percentage of EdU-positive cells was calculated using the following formula: (EdU-stained cells/Hoechst-stained cells)×100%. The assay was performed in three replicate wells.

2.6 Cell viability assay

A total of 3×10^3 cells were seeded into each well of a 96-well plate. Then, 10 μL of cell counting kit-8 (CCK-8) reagent (CA1210; Solarbio, Beijing, China) was added into each well on Days 0, 1, 2, and 3. After 2 h of incubation, the absorbance at 450 nm was measured by using an Infinite M200 PRO NanoQuant microplate reader (TECAN, Switzerland). The mean value of absorbance was calculated from three replicate wells.

2.7 Plate colony formation assay

A total of 1×10^3 cells/well were cultured in a six-well plate for about two weeks with a change of medium every 3 d. Then, the colonies underwent fixation with 4% paraformaldehyde and staining with 0.1% (1 g/L) crystal violet. The following formula was applied to estimate the rate of plate colony formation: (colonies number/1000)×100%.

2.8 Sphere formation assay

Single-cell suspension was prepared in serum-free DMEM/F12 medium (C11330500BT; Gibco, Shanghai,

China) supplemented with 20 ng/mL epidermal growth factor (HY-P7109; MCE, Shanghai, China) and 10 ng/mL basic fibroblast growth factor (HY-P7004; MCE). The cells were then plated in ultra-low attachment six-well plates (3471; Corning) at a density of 2000 cells/well. The plates were gently settled in an incubator for two weeks. Spheres more than 75 μm were counted and the following formula was applied to calculate the rate of sphere formation: (sphere number/2000)×100%.

2.9 Wound healing assay

Cells were seeded in six-well plates and were grown to confluence. A standardized wound was introduced by scratching the monolayer with a sterile 200 μL pipette tip. After scratching, cells were washed with PBS and captured using a microscope with the MShot Image Analysis System (MShot, Guangzhou, China). Then, a medium containing 1% (volume fraction) serum was added to each well. After 24 h of incubation, wound images were captured to document the closure rate. The relative closure rate was calculated by the formula: 100%−(wound area after 24 h/initial wound area)×100%.

2.10 Transwell assay

Transwell chambers (3422; Corning) with uncoated upper surfaces and those precoated with BD Matrigel Matrix (356234; Beijing Biolead Biology Sci & Tech, Beijing, China) were used for the migration and invasion assays, respectively. Cell suspension (4×10^4 cells into 200 μL serum-free DMEM) was planted on the upper surface of the chamber. Then, the chamber was placed into a 24-well plate with each well containing 600 μL of DMEM medium with 10% FBS for 48 h. The cells were fixed in 4% paraformaldehyde for 15 min, permeabilized by methanol for 15 min, and then stained with 0.1% crystal violet overnight. After removing non-migrating or non-invading cells, the staining images were captured using a microscope with the MShot Image Analysis System. Three random fields of each chamber were selected to quantify the migrating or invading cells.

2.11 Reverse transcription-quantitative polymerase chain reaction (RT-qPCR)

Total RNA from cultured cells was extracted using the RNA-Quick Purification Kit (DP419; TIANGEN, Beijing, China) following the instructions and then subject to concentration detection using the NanoDrop 2000 spectrophotometer (Thermo Fisher Scientific, USA). Extracted RNA (1 μg) was utilized to synthesize complementary DNA (cDNA) using the LunaScript™ RT SuperMix Kit (E3010; NEB, Beijing, China). Then, quantitative polymerase chain reaction (qPCR) was carried out using the Power SYBR® Green Master Mix (4367659, Thermo Fisher Scientific) on the QuantStudio™ 5 System (Thermo Fisher Scientific). The glyceraldehyde-3-phosphate dehydrogenase (*GAPDH*) messenger RNA (mRNA) expression was detected as the internal control. The analytic method of $2^{-\Delta\Delta C_T}$ was applied to calculate the relative mRNA levels of target genes. Detailed information about primer sequences is summarized in Table S1.

2.12 Western blot analysis

Total proteins from cells were harvested with the lysis buffer consisting of 10 mmol/L of Tris-HCl (pH 7.4), 1% (0.01 g/mL) of sodium dodecyl sulfate (SDS), and 1 mmol/L of Na_3VO_4. Then, the concentration of extracted protein was measured using a NanoDrop 2000 spectrophotometer (Thermo Fisher Scientific). For the extraction of cytoplasmic and nuclear proteins, the Minute™ Cytoplasmic and Nuclear Extraction Kit for Cells (SC-003; Invent, Beijing, China) was applied to lyse cells according to the instructions, followed by concentration measurement via the BCA Protein Assay Kit (WB6501; NCM Biotech). Equivalent amounts of cell proteins were separated using sodium dodecyl sulfate-polyacrylamide gel electrophoresis (SDS-PAGE) and then transported to nitrocellulose membranes (HATF00010; Merck Millipore, Beijing, China). After being blocked in Tris-buffered saline (TBS) with 5% (volume fraction) skim milk, the membranes were washed three times in TBS and incubated with primary antibodies at 4 °C overnight, followed by incubation with corresponding secondary antibodies for 1 h at room temperature. The signals from target proteins were detected using an enhanced chemiluminescence (ECL) system (WBKLS0500; Merck Millipore) and the Tanon Imaging System (Tanon, China). The protein levels from three independent experiments were quantified using the ImageJ software (Schneider et al., 2012). Antibodies used here are listed in Table S2. The full and uncropped western blots were present in the supplementary data (raw data for western blot).

2.13 Immunofluorescence (IF) assay

A total of 150000 cells suspended in 3 mL of medium were added into the Glass Bottom Cell Culture Dish (BS-15-GJM; Biosharp, Anhui, China) to grow for 24 h. Then, the cells were fixed with 4% paraformaldehyde for 10 min, permeabilized by 0.3% Triton X-100 for 10 min, and blocked by 5% BSA for 1 h. The cells were incubated with indicated primary antibodies at 4 °C overnight followed by corresponding fluorescence-conjugated secondary antibodies. After the treatment with an antifade mountant containing 4',6-diamidino-2-phenylindole (DAPI) (Solarbio, S2110), images were captured by a confocal laser-scanning microscope (LSM 800, Zeiss, Germany). The antibodies used for immunofluorescence (IF) are summarized in Table S2.

2.14 RNA sequencing

Total RNAs from HEECs or HEEC-Cr(VI) cells were extracted from three duplicate wells in six-well plates with TRNzol universal agent (DP424; TIANGEN) and sent to Novogene (Beijing, China) for RNA sequencing (RNA-Seq). RNA qualification was detected using the Bioanalyzer 2100 system (Agilent Technologies, CA, USA). After constructing libraries with the NEBNext® Ultra™ RNA Library Prep Kit for Illumina® (NEB, E7530), we performed sequencing with the Illumina NovaSeq 6000 (Illumina, USA) following the 150 bp paired-end strategy. Paired-end clean reads obtained from raw data (FASTQ sequence files) were aligned to the *Homo sapiens* (GRCh38/hg38) by using HISAT2 (v2.0.5) (https://daehwankimlab.github.io/hisat2). Gene expression levels were normalized as fragments per kilobase of transcript per million base pairs sequenced. DESeq2 R package (v1.16.1) was adopted to analyze the differentially expressed genes (DEGs) between HEEC-Cr(VI) and HEEC groups with the criteria of $|\log_2(\text{fold change})|>1$ and adjusted P-value<0.05 (Love et al., 2014). The Gene Ontology (GO) analysis of the DEGs was plotted using an online platform (https://www.bioinformatics.com.cn; last accessed on Nov. 10, 2023) for data analysis and visualization (Tang et al., 2023). Gene set enrichment analysis (GSEA) was performed using GSEA software (Subramanian et al., 2005).

2.15 Statistical analysis

Statistical analyses were conducted using the Prism software version 8.0.1 (GraphPad, USA). All experiments were performed independently at least three times unless noted. The two-way analysis of variance (ANOVA) test was performed for the statistical analyses of cell vitality assays and growth curves of xenograft tumors, while other differences between any two groups were determined using the paired or unpaired t-test. Measurement data are presented as mean±standard deviation (SD). When the P-value is less than 0.05, differences are considered significant.

3 Results

3.1 HEECs acquiring malignant proliferation and stemness phenotypes after chronic Cr(VI) exposure

As shown in Fig. 1a, the half maximal inhibitory concentration (IC_{50}) value of Cr(VI) for 24 or 48 h of treatment is 7.198 or 4.208 μmol/L in HEECs. To explore the potential effects of chronic exposure to Cr(VI) on the initiation of EC, we continuously cultured HEECs in the medium with 0.25 μmol/L of Cr(VI) for 60 generations for approximately six months and then obtained the transformed cell line, named HEEC-Cr(VI) (Fig. 1b). The anchorage-independent growth in soft agar has been considered a key phenomenon for the malignant transformation of normal cells (Freedman and Shin, 1974; Shin et al., 1975). Our results revealed that HEEC-Cr(VI) cells formed obvious colonies in soft agar while HEECs can hardly proliferate under the same conditions (Fig. 1c), which suggests that HEEC-Cr(VI) cells are derived from the malignant transformation of their parental cells. To determine the proliferative capacity of HEEC-Cr(VI) cells, we performed the assays of EdU incorporation, CCK-8, and plate colony formation. Our results demonstrated an enhanced proliferation of HEEC-Cr(VI) cells when compared to HEECs (Figs. 1d–1f). The acquisition of malignantly proliferative potential is usually accompanied by an increase in cell stemness (Aponte and Caicedo, 2017; Jing et al., 2021). As expected, a sphere formation assay revealed a significantly enhanced stemness in HEEC-Cr(VI) cells (Fig. 1g), which was further supported by increased protein levels of cellular-myelocytomatosis viral oncogene (c-Myc) and sex-determining region Y-box 2 (SOX-2), markers for cell stemness (Figs. 1h and S1). To evaluate the tumorigenicity of HEEC-Cr(VI) cells in vivo, subcutaneous

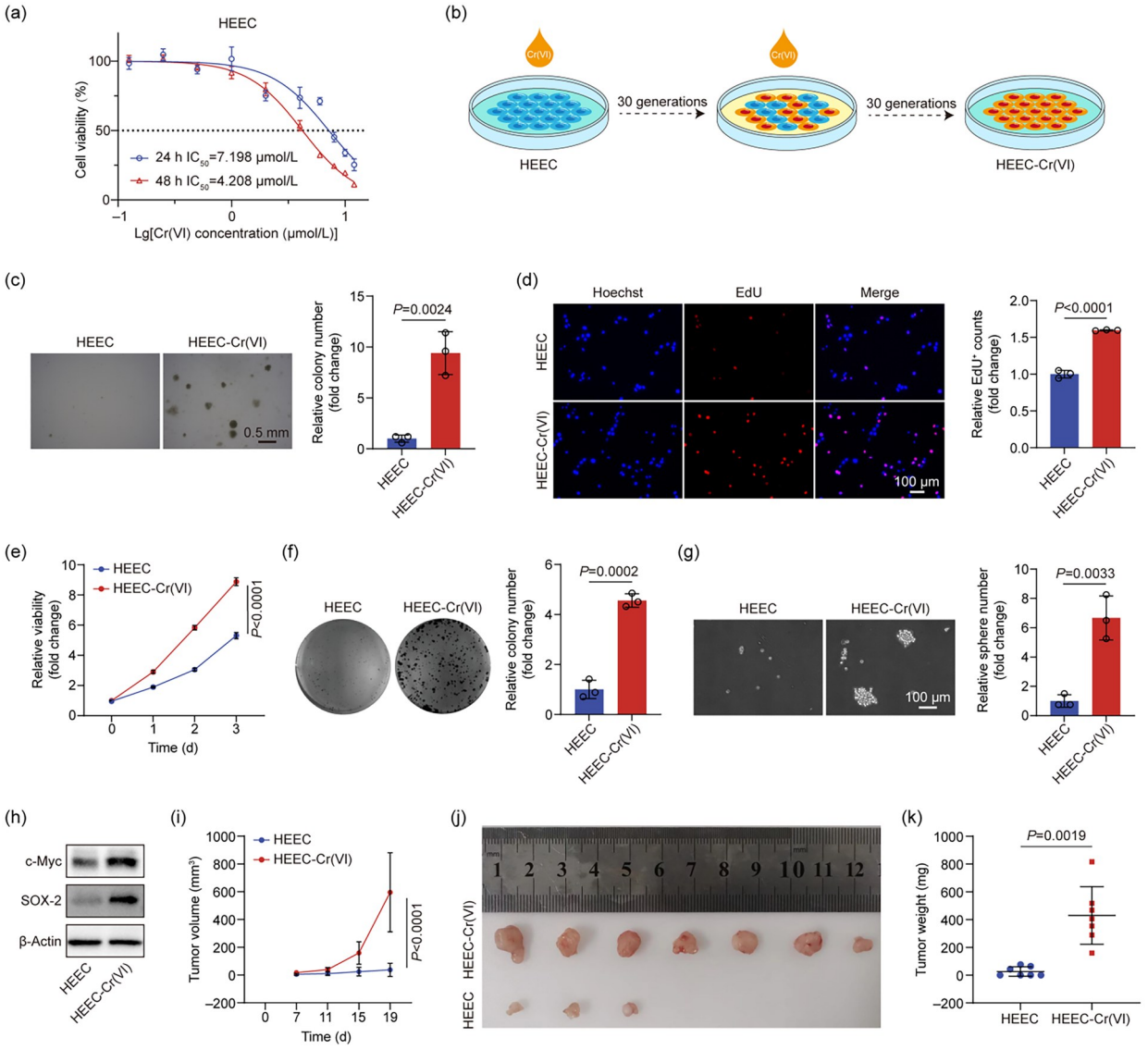

Fig. 1 Human esophageal epithelial cells (HEECs) acquiring malignant proliferation in vitro and in vivo after chronic Cr(VI) exposure. (a) HEECs were treated with different doses of Cr(VI) for 24 or 48 h and then subjected to cell viability detection via cell counting kit-8 (CCK-8) assays. The fitting curves were performed to calculate and plot the half maximal inhibitory concentration (IC_{50}) values. (b) Schematic diagram clarifying the establishment of Cr(VI)-induced malignantly transformed HEECs, named HEEC-Cr(VI). (c) A soft agar colony formation assay was applied to evaluate the anchorage-independent growth of HEECs and HEEC-Cr(VI) cells (*n*=3). (d–f) The proliferation of HEECs and HEEC-Cr(VI) cells was assessed using the 5-ethynyl-2-deoxyuridine (EdU) incorporation (*n*=3) (d), CCK-8 (*n*=3) (e), and plate colony formation assays (*n*=3) (f). (g) A sphere formation assay was applied to evaluate the stemness of HEECs and HEEC-Cr(VI) cells. Representative images with a scale bar and their quantification are displayed (*n*=3). (h) The protein levels of cellular-myelocytomatosis viral oncogene (c-Myc) and sex-determining region Y-box 2 (SOX-2) were detected using western blot. β-Actin was used as a loading control. (i–k) BALB/c nude mice (*n*=7) were subcutaneously xenografted with HEECs or HEEC-Cr(VI) cells for 19 d. Tumor growth curve (i), the image of xenografts (j), and quantification for tumor weights (k) are shown. All data for statistical analysis are displayed as mean±standard deviation (SD). Statistical significance was determined by performing an unpaired *t*-test (c, d, f, g, k) or a two-way analysis of variance (ANOVA) (e, i).

formation of xenograft in BALB/c nude mice was performed. Consistent with the phenotypes in vitro, HEEC-Cr(VI) cells, but not their parental cells (HEECs), displayed a significant ability to xenograft subcutaneously (Figs. 1i–1k). Together, these results suggest that chronic exposure to Cr(VI) induced HEECs to acquire malignantly proliferative capacity and stemness.

3.2 Attenuated motility and enhanced adhesion in HEEC-Cr(VI) cells

To explore the cellular motility of HEEC-Cr(VI), we conducted wound healing assays and found the migration capacity of HEEC-Cr(VI) cells was weakened compared to HEECs (Fig. 2a). Similarly, transwell assays revealed that the migration and invasion of HEEC-Cr(VI) cells were attenuated compared with HEECs (Fig. 2b). Additionally, when digested by trypsin, HEEC-Cr(VI) cells took more time to detach from the culture dish compared to HEECs (Fig. 2c). In line with the weakened cell migration and invasion, HEEC-Cr(VI) cells exhibited an increased level of E-cadherin and a reduced matrix metalloproteinase-2 (MMP-2) protein expression when compared to HEECs (Figs. 2d and S2). However, we did not observe distinct differences in the morphology of the two types of cells (Fig. 2e). Collectively, HEEC-Cr(VI) cells possess the characteristics of weaker cell motility and stronger cell adhesion than their parental cells.

3.3 Lack of HEEC-Cr(VI) characteristics in HEECs with Cr(VI) acute exposure

To determine whether the phenotypes of malignant proliferation and stemness in HEEC-Cr(VI) cells are from the transformation induced by chronic Cr(VI) exposure or from Cr(VI) itself, HEECs were treated with 0.25 μmol/L of Cr(VI) for 48 h. Our results demonstrated that HEECs with acute treatment of Cr(VI) failed to form colonies in soft agar (Fig. 3a). Similarly, EdU incorporation or CCK-8 assays revealed no prominent difference in proliferative capacity in HEECs between acute exposure to Cr(VI) and vehicle control groups (Figs. 3b and 3c), while plate colony formation assays displayed a reduced number of colonies from HEECs with acute exposure to Cr(VI) (Fig. 3d). Interestingly, although acute exposure to Cr(VI) had no effects on the stemness of HEECs, the protein levels of c-Myc and SOX-2 displayed a slight decrease upon the treatment of Cr(VI) for 48 h (Figs. 3e, 3f, S3a, and S3b). In addition, wound healing and transwell

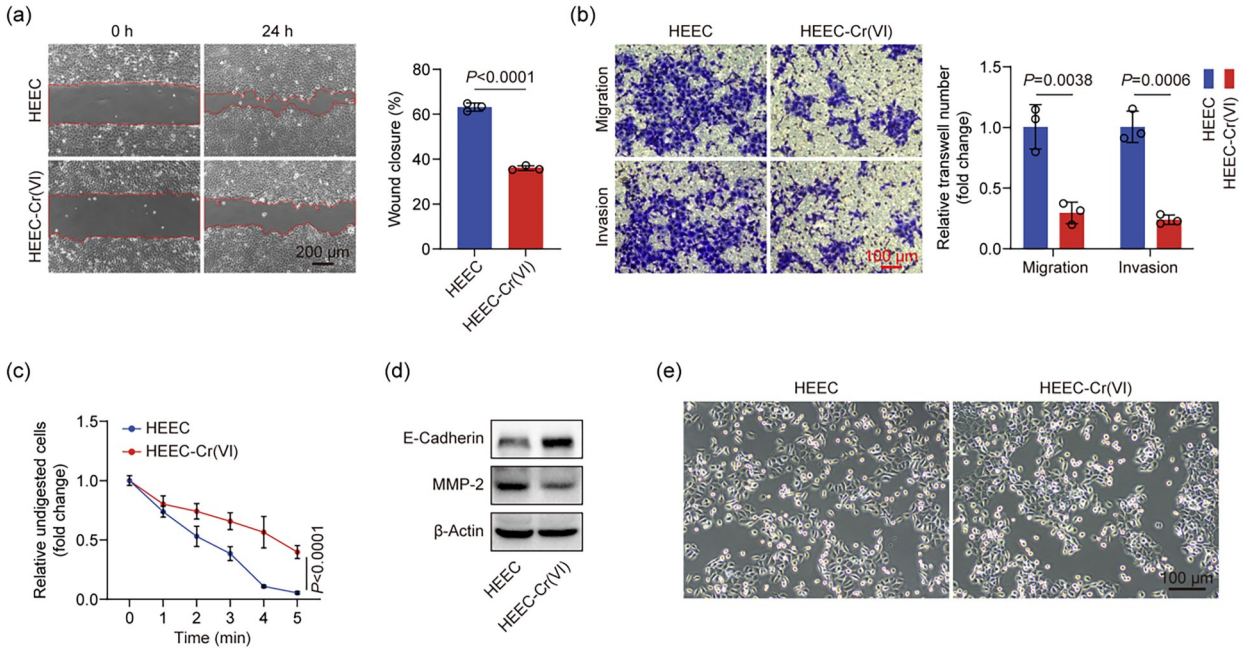

Fig. 2 Attenuated motility and enhanced adhesion in Cr(VI)-induced malignantly transformed human esophageal epithelial cells (HEEC-Cr(VI) cells). (a) Wound healing assays were performed for the migration capacity of HEECs and HEEC-Cr(VI) cells (*n*=3). (b) The ability of cell migration and invasion was evaluated using a transwell assay (*n*=3). (c) HEECs and HEEC-Cr(VI) cells were subjected to the digestion of trypsin for the indicated time. Then, adherent cells were counted (*n*=3). (d) Western blot analysis was applied to detect the protein levels of E-cadherin and matrix metalloproteinase-2 (MMP-2) in HEECs and HEEC-Cr(VI) cells. β-Actin protein was applied as a loading control. (e) The morphological characteristics of HEECs and HEEC-Cr(VI) cells under an inverted microscope. All data for statistical analysis are presented as mean±standard deviation (SD). An unpaired *t*-test was used to determine the statistical significance in (a, b), while the two-way analysis of variance (ANOVA) was used in (c).

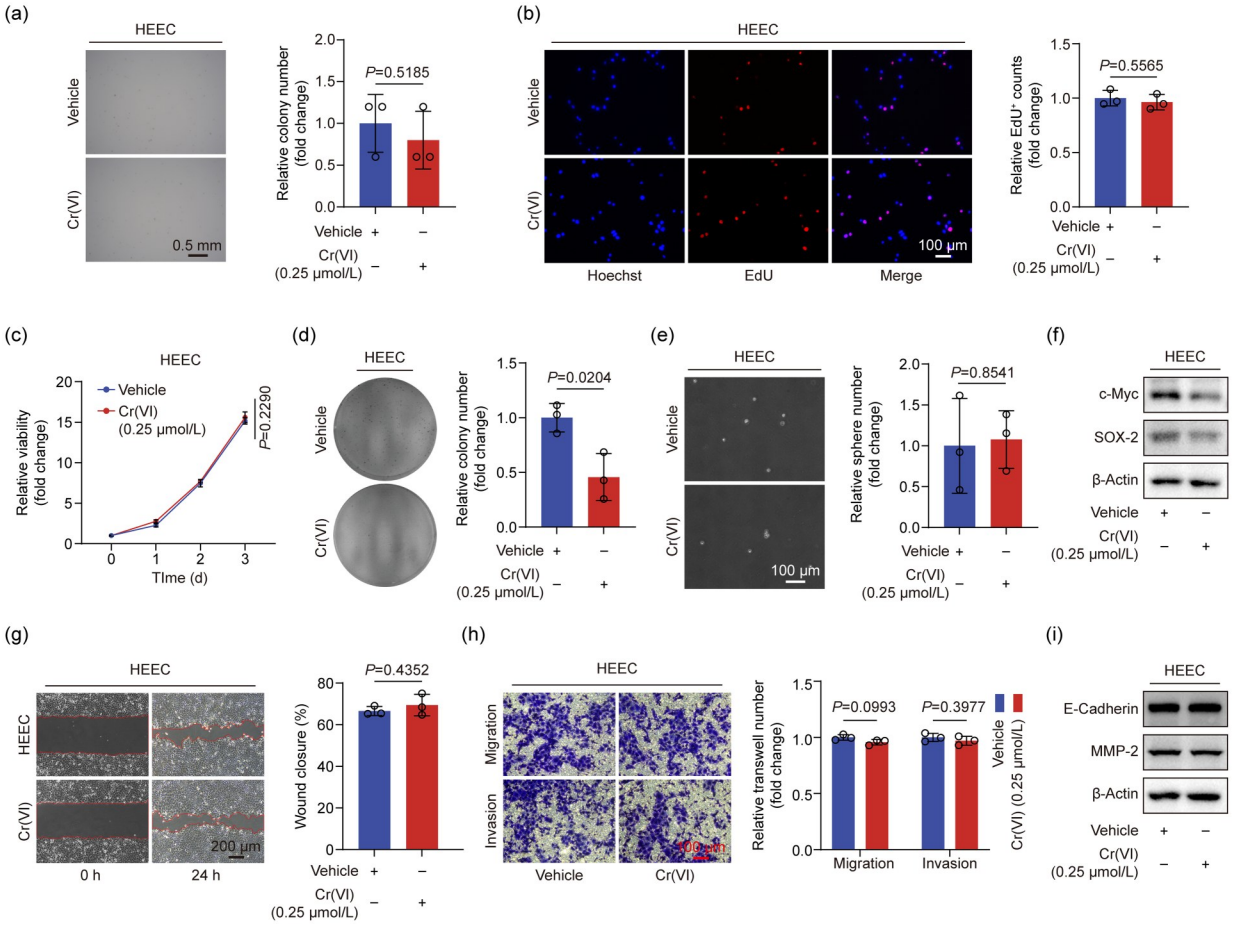

Fig. 3 Lacking the characteristics of Cr(VI)-induced malignantly transformed human esophageal epithelial cells (HEEC-Cr(VI) cells) in HEECs with Cr(VI) acute exposure. (a) HEECs were treated with Cr(VI) (0.25 μmol/L) or vehicle control for 48 h, followed by soft agar colony formation assays to assess cell anchorage-independent growth (*n*=3). (b–d) The 5-ethynyl-2-deoxyuridine (EdU) incorporation (*n*=3) (b), cell counting kit-8 (CCK-8) (*n*=3) (c), and plate colony formation assays (*n*=3) (d) were performed to detect the proliferative capacity of HEECs with or without exposure to Cr(VI) (0.25 μmol/L) for 48 h. (e) HEECs were treated with Cr(VI) (0.25 μmol/L) for 48 h or not, followed by a sphere formation assay to evaluate the stemness. Representative images with a scale bar and their quantification are indicated (*n*=3). (f) Western blot analysis was performed to determine sex-determining region Y-box 2 (SOX-2) and cellular-myelocytomatosis viral oncogene (c-Myc) protein levels in HEECs treated with Cr(VI) (0.25 μmol/L) for 48 h or not. Loading control for western blot refers to β-actin protein levels. (g, h) The wound healing (*n*=3) (g) and transwell assays (*n*=3) (h) were used to evaluate the migration and invasion of HEECs with or without acute exposure (48 h) to Cr(VI) (0.25 μmol/L). (i) E-Cadherin and matrix metalloproteinase-2 (MMP-2) proteins were detected in HEECs with acute exposure (48 h) to Cr(VI) (0.25 μmol/L) or not using western blot. β-Actin protein levels were applied for loading control. The data for statistical analysis are indicated as mean±standard deviation (SD). Statistical significance was identified by applying an unpaired *t*-test (a, b, d, e, g, h) or the two-way analysis of variance (ANOVA) (c).

assays revealed that acute exposure to Cr(VI) displayed no alteration in the motility of HEECs (Figs. 3g and 3h). Consistently, there was no change in protein levels of E-cadherin or MMP-2 upon 48 h of exposure to Cr(VI) (Figs. 3i, S3c, and S3d). Together, these results support the suggestion that the biological characteristics, especially the malignant proliferation and stemness, of HEEC-Cr(VI) cells are derived from Cr(VI)-induced transformation but not from Cr(VI) itself.

3.4 Abnormal activation of Notch signaling pathway in HEEC-Cr(VI) cells

To explore potential mechanisms responsible for HEECs' malignant transformation induced by chronic exposure to Cr(VI), we applied RNA-Seq to obtain gene expression profiles from HEEC-Cr(VI) cells and HEECs. As shown in Fig. 4a, when compared to HEECs, a total of 2381 DEGs (1447 upregulated and

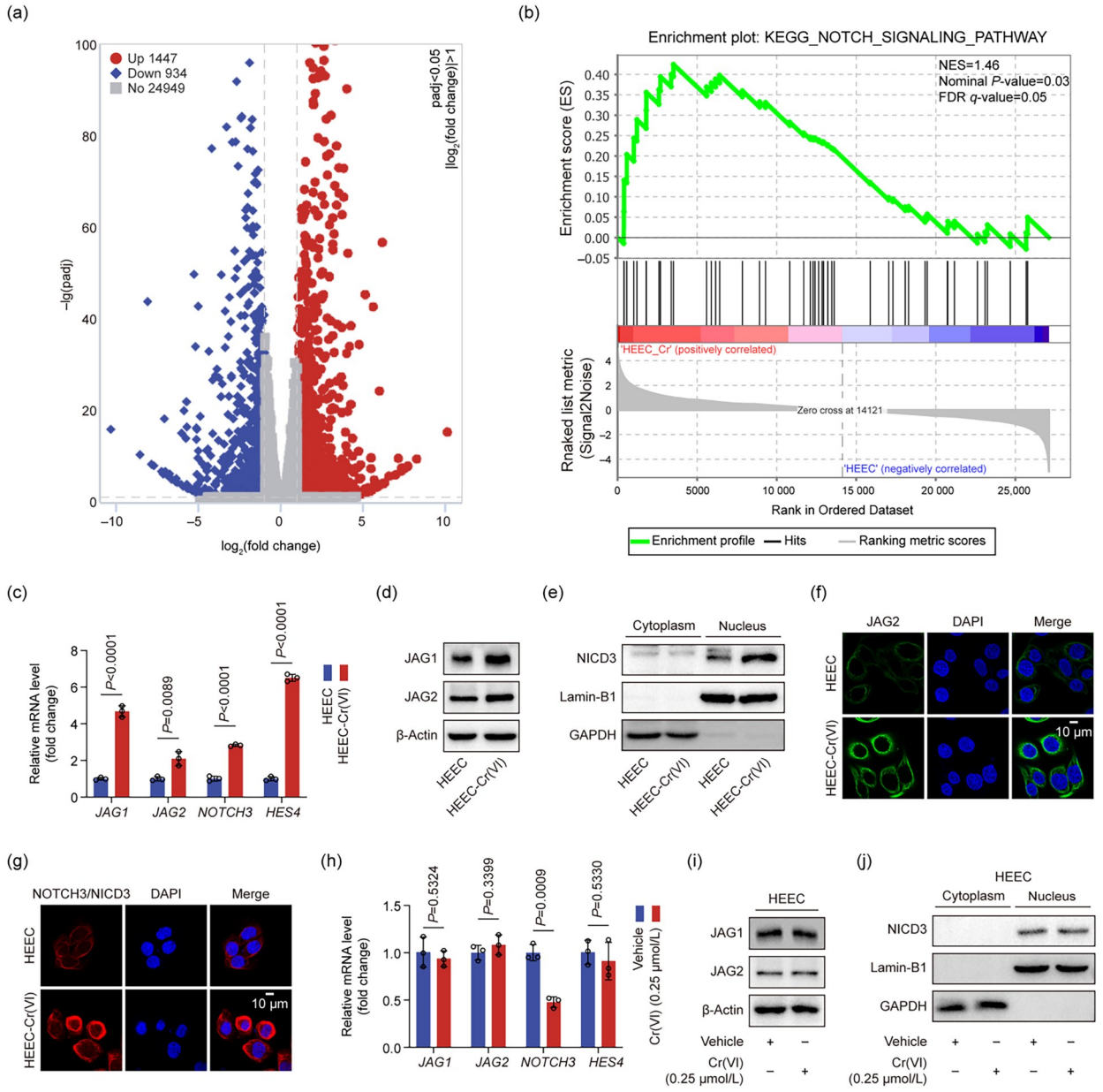

Fig. 4 Abnormal activation of Notch signaling pathway in Cr(VI)-induced malignantly transformed human esophageal epithelial cells (HEEC-Cr(VI) cells). (a) The volcano diagram was applied to show differentially expressed genes (DEGs) between HEEC-Cr(VI) cells and HEECs according to the data from RNA sequencing (RNA-Seq). HEECs were used as the control group. (b) Gene set enrichment analysis (GSEA) was conducted to evaluate the status of the Notch signaling pathway in HEEC-Cr(VI) cells. (c) The messenger RNA (mRNA) levels of Jagged 1 (*JAG1*), *JAG2*, *NOTCH3*, and hairy/enhancer of split 4 (*HES4*) in HEECs and HEEC-Cr(VI) cells were detected using reverse transcription-quantitative polymerase chain reaction (RT-qPCR). The glyceraldehyde-3-phosphate dehydrogenase (*GAPDH*) mRNA levels were used as an internal control. (d) JAG1 and JAG2 protein levels in HEECs and HEEC-Cr(VI) cells were determined by western blot analysis. (e) Cytoplasmic and nuclear proteins from HEECs or HEEC-Cr(VI) cells were extracted and then subjected to western blot for detecting active truncate of NOTCH3 protein (NICD3) levels. (f, g) Subcellular locations of JAG2 (f) and NOTCH3/NICD3 proteins (g) were identified using immunofluorescence (IF) assays. (h–j) HEECs were treated with 0.25 μmol/L of Cr(VI) or vehicle control for 48 h, followed by RT-qPCR to detect *JAG1*, *JAG2*, *NOTCH3*, and *HES4* mRNA levels (h) and by western blot to evaluate protein levels of JAG1, JAG2 (i), and NICD3 (j). The loading control for the nuclear or cytoplasmic protein lysate was referred by Lamin-B1 or GAPDH protein levels. The data in (c, h) are indicated as mean±standard deviation (SD) (n=3), and the statistical significance for the difference was identified using an unpaired t-test. padj: adjusted P-value.

934 downregulated genes) were identified in HEEC-Cr(VI) cells following the conditions of adjusted *P*-value<0.05 and $|\log_2(\text{fold change})|>1$. The GO analysis based on upregulated DEGs revealed the association with the terms of epidermis development and transcriptional activity, while downregulated DEGs showed a close correlation to the extracellular matrix and cell migration (Fig. S4), which is consistent with the enhanced proliferation and attenuated mobility of HEEC-Cr(VI) cells. Since HEEC-Cr(VI) cells acquired malignant proliferation and stemness, we further analyzed the related signaling pathways, including Wnt, Hedgehog, and Notch. GSEA results revealed abnormal activation of the Notch signaling pathway, an obvious inhibition of the Wnt signaling, and no significant alterations of the Hedgehog pathway in HEEC-Cr(VI) (Figs. 4b and S5). To verify the results from RNA-Seq, we performed reverse transcriptase-qPCR (RT-qPCR) to detect the mRNA levels of the Notch signaling ligands (Jagged 1 (*JAG1*) and *JAG2*), receptor (*NOTCH3*), and downstream target (hairy/enhancer of split 4 (*HES4*)), and determined their upregulation at the mRNA level in HEEC-Cr(VI) cells (Fig. 4c). Similarly, upregulated JAG1 and JAG2 protein levels and increased nucleus accumulation of active truncate of NOTCH3 protein (NICD3) were found in HEEC-Cr(VI) cells (Figs. 4d, 4e, and S6). Additionally, IF assays revealed the increased JAG2 and NOTCH3 proteins in cell membranes and the accumulation of nucleus NICD3 protein in HEEC-Cr(VI) cells (Figs. 4f and 4g). These results confirm the aberrant activation of the Notch signaling in HEEC-Cr(VI) cells. Interestingly, bioinformatics analysis based on Gene Expression Omnibus (GEO) datasets (GSE130078) (You et al., 2019) and The Cancer Genome Atlas (TCGA) database from the University of California Santa Cruz (UCSC) Xeno platform (Goldman et al., 2020) showed that mRNA levels of components in the Notch pathway are upregulated in ESCC (Fig. S7), which further supports the potentially key role of the Notch signaling during Cr(VI)-induced malignant transformation of HEECs.

To rule out the possibility that the activated Notch signaling pathway is directly caused by Cr(VI) itself, HEECs were exposed to 0.25 μmol/L of Cr(VI) for 48 h and were then subject to the detection of *JAG1*, *JAG2*, *NOTCH3*, and *HES4* expression levels. As shown in Fig. 4h, the *JAG1*, *JAG2*, or *HES4* mRNA level showed no obvious alteration in HEECs upon acute exposure to Cr(VI), while *NOTCH3* mRNA expression was significantly decreased. Consistently, the treatment of Cr(VI) (0.25 μmol/L) for 48 h did not affect the protein level of JAG1 or JAG2 (Figs. 4i, S8a, and S8b). It should be noted that nucleus accumulation of NICD3 protein was not altered in HEECs upon acute exposure to Cr(VI) (0.25 μmol/L) (Figs. 4j and S8c). Taken together, these results indicate that aberrant activation of the Notch signaling pathway is the property of HEEC-Cr(VI) cells but not the consequence directly caused by Cr(VI).

3.5 Impaired malignant proliferation and stemness in HEEC-Cr(VI) cells upon Notch signaling pathway blockage

To identify the function of the Notch signaling pathway in the malignant phenotypes of HEEC-Cr(VI) cells, the *N*-[*N*-(3,5-difluorophenacetyl)-L-alanyl]-*S*-phenylglycine *t*-butyl ester (DAPT), a potent inhibitor against the Notch signaling pathway, was applied. Unsurprisingly, DAPT treatment not only decreased NICD3 protein levels in the nucleus but also downregulated *HES4* mRNA expression in HEEC-Cr(VI) cells (Figs. 5a, 5b, and S9a). Then, we evaluated the malignantly proliferative capacity of HEEC-Cr(VI) cells treated with DAPT or vehicle control. Interestingly, DAPT treatment remarkedly diminished the anchorage-independent growth of HEEC-Cr(VI) cells in soft agar (Fig. 5c). In addition, DAPT-induced inhibition on malignant proliferation of HEEC-Cr(VI) cells was further confirmed by reduced EdU incorporation, attenuated cell viability, and impaired formation of plate colonies (Figs. 5d–5f). Similarly, sphere formation assays revealed that the stemness of HEEC-Cr(VI) cells was significantly impaired by DAPT treatment (Fig. 5g). Further detection on c-Myc and SOX-2 proteins demonstrated that DAPT treatment markedly downregulated c-Myc expression but had no effect on SOX-2 protein levels (Figs. 5h, S9b, and S9c), which indicates that other pathways are involved in SOX-2 upregulation in HEEC-Cr(VI) cells. In addition, we explored whether the activated Notch signaling pathway regulates the weakened mobility of HEEC-Cr(VI) cells. Wound healing and transwell assays revealed that the migration and invasion of HEEC-Cr(VI) cells were not altered by DAPT (Figs. 5i and 5j). Conformably, DAPT treatment did not affect E-cadherin or

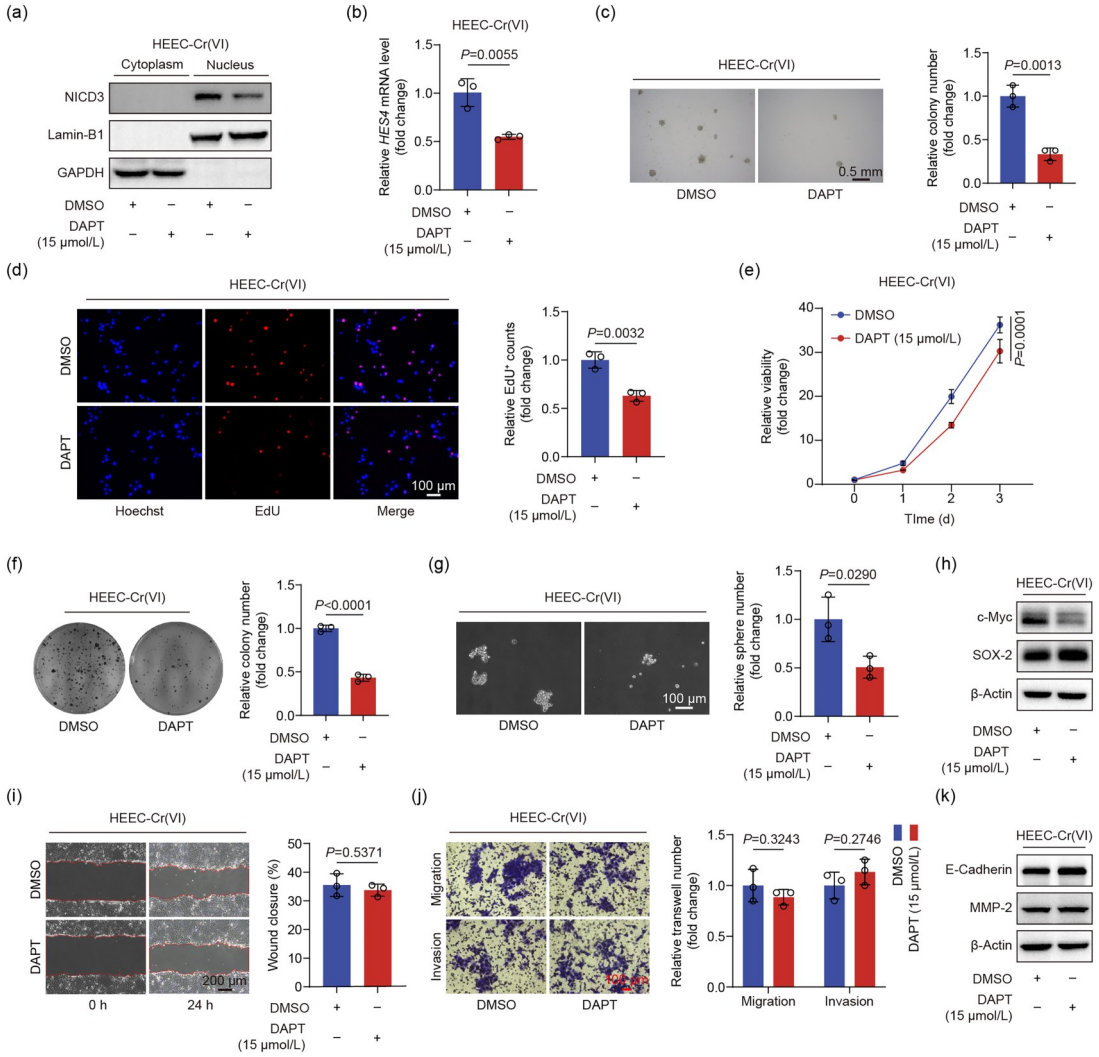

Fig. 5 Impaired malignant proliferation and stemness in Cr(VI)-induced malignantly transformed human esophageal epithelial cells (HEEC-Cr(VI) cells) upon Notch signaling pathway blockage. (a, b) HEEC-Cr(VI) cells were treated with *N*-[*N*-(3,5-difluorophenacetyl)-L-alanyl]-*S*-phenylglycine *t*-butyl ester (DAPT) (15 μmol/L), a potent inhibitor against the Notch signaling pathway, or vehicle control for 48 h and then subjected to western blot to assess the protein level of active truncate of NOTCH3 protein (NICD3) (a) and reverse transcription-quantitative polymerase chain reaction (RT-qPCR) to determine hairy/enhancer of split 4 (*HES4*) messenger RNA (mRNA) level (b). Lamin-B1 and glyceraldehyde-3-phosphate dehydrogenase (GAPDH) protein were respectively used as a loading control for the nuclear and cytoplasmic protein lysates. The *GAPDH* mRNA level was applied as an internal control for RT-qPCR. (c) The anchorage-independent growth of HEEC-Cr(VI) cells in DAPT (15 μmol/L) or vehicle control groups was evaluated by soft agar colony formation assays. The treatment of DAPT (15 μmol/L) continued throughout the whole process of experiments (three weeks). (d, e) HEEC-Cr(VI) cells were treated with DAPT (15 μmol/L) or vehicle control for 48 h. Then, the proliferation of treated cells was evaluated by the 5-ethynyl-2-deoxyuridine (EdU) incorporation (d) and cell counting kit-8 (CCK-8) (e). (f) Plate colony formation assays were applied to evaluate the proliferation of HEEC-Cr(VI) cells treated with DAPT (15 μmol/L) or vehicle control. DAPT (15 μmol/L) treatment continued throughout the whole process of plate colony formation assays (two weeks). (g) A sphere formation assay was used to assess the stemness of HEEC-Cr(VI) cells treated with DAPT (15 μmol/L) or vehicle for the whole experimental process (two weeks). Representative images with a scale bar and their quantification are shown. (h) HEEC-Cr(VI) cells were treated with DAPT (15 μmol/L) or vehicle for 48 h, and then subjected to western blot analysis to detect sex-determining region Y-box 2 (SOX-2) and cellular-myelocytomatosis viral oncogene (c-Myc) protein levels. β-Actin protein was applied as a loading control. (i, j) After treating HEEC-Cr(VI) cells with DAPT (15 μmol/L) or vehicle for 48 h, the wound healing (i) and transwell assays (j) were applied to assess cell migration and invasion. (k) Western blot analysis was used to detect the protein levels of E-cadherin and matrix metalloproteinase-2 (MMP-2) in HEEC-Cr(VI) cells treated with DAPT (15 μmol/L) or vehicle for 48 h. All data in (b–g, i, j) for statistical analysis are displayed as mean±standard deviation (SD) (*n*=3). An unpaired *t*-test was applied to identify the statistical significance in (b, c, d, f, g, i, j), while the two-way analysis of variance (ANOVA) was used in (e).

MMP-2 protein level (Figs. 5k, S9d, and S9e). Collectively, these results suggest that the activation of the Notch signaling pathway is essential to maintain the malignant proliferation and stemness in HEEC-Cr(VI) cells.

4 Discussion

Cr(VI) contaminations via inhalation, drinking water, and food are deeply associated with the morbidity of many human cancers, which pose a huge threat to human health (Sun et al., 2015; Chen et al., 2019; Iyer et al., 2023). However, the exact function of Cr(VI) in esophageal tumorigenesis and the molecular mechanism underlying the initiation of Cr(VI)-associated EC remain largely unknown. Here, we found that HEECs with long-term exposure to Cr(VI) obtained the capability of anchorage-independent growth in soft agar and subcutaneous xenograft in BALB/c nude mice as well as stemness, among which, abnormally activated Notch signaling induced by chronic exposure to Cr(VI) is responsible for the maintenance of malignant proliferation and stemness in HEEC-Cr(VI) cells (Fig. 6).

To determine the function of chronic exposure to Cr(VI) in the occurrence of EC, HEECs were continuously cultured in the medium with Cr(VI) (0.25 μmol/L) for approximately six months to establish the transformed cell line, HEEC-Cr(VI). The in vitro and in vivo experiments demonstrated that HEEC-Cr(VI) cells can anchorage-independently grow in soft agar and subcutaneously xenograft in BALB/c nude mice, which suggests Cr(VI)-induced malignant transformation of HEECs. Interestingly, HEEC-Cr(VI) cells exhibit enhanced cell adhesion and attenuated cell motility compared to their parental cells, HEECs, which was further supported by upregulated E-cadherin and

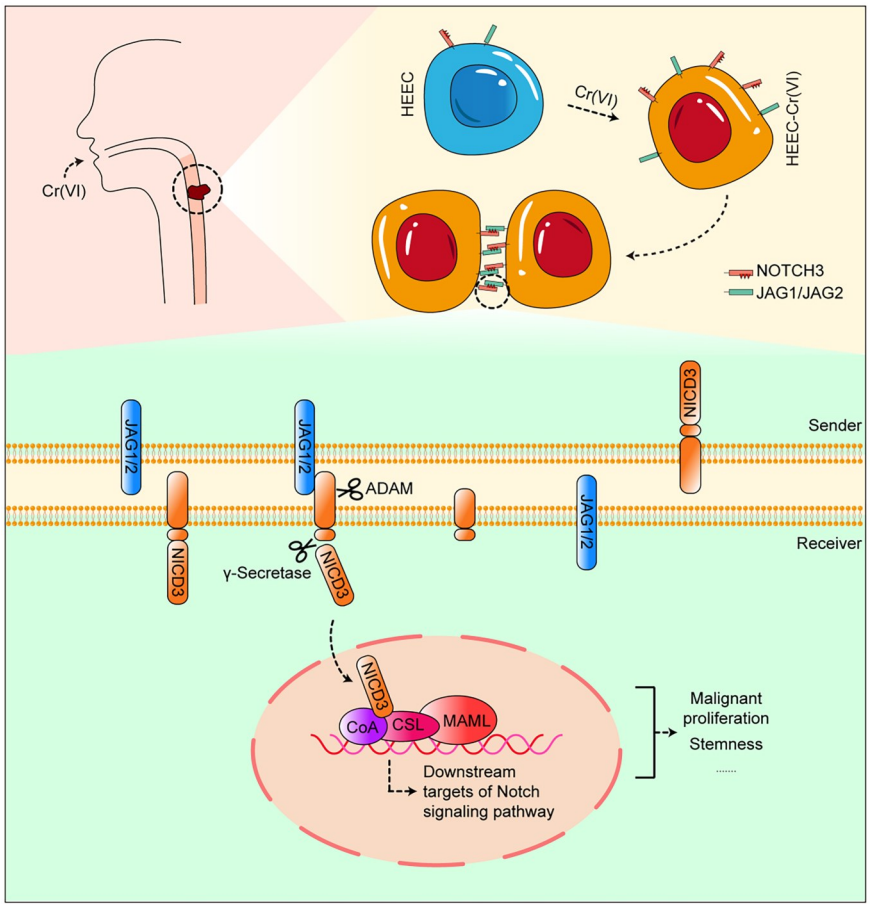

Fig. 6 Schematic diagram elucidating the regulatory mechanism underlying the Cr(VI)-induced esophageal tumorigenesis. HEEC: human esophageal epithelial cell; JAG: Jagged; NICD3: active truncate of NOTCH3 protein; CoA: coenzyme A; CSL: CBF1, Suppressor of Hairless, Lag-1; MAML: mastermind-like.

downregulated MMP-2 in HEEC-Cr(VI) cells. Consistent with our finding, the study by Sun et al. (2011) reported that genes related to cell junction are significantly increased in Cr(VI)-induced transformed BEAS-2B cells. It is noteworthy that altered E-cadherin protein levels usually indicate epithelial–mesenchymal transition (EMT) (Brabletz et al., 2021). However, no obvious differences in morphology were found in HEEC-Cr(VI) cells. Some studies have reported that chromium exposure is closely associated with the incidence of ESCC (Amer et al., 1990; Hashemian et al., 2017). Interestingly, HEEC-Cr(VI) cells display increased expression of SOX-2, a marker related to squamous cell carcinoma (Hsieh et al., 2019), compared to HEECs. In summary, these results demonstrate that HEECs possess malignantly proliferative capacity after chronic exposure to Cr(VI). It should be pointed out that introducing another cell line for the establishment of Cr(VI)-induced transformed cells in our further study may help to identify the HEEC-specific phenotypes, although HEECs were recommended as an excellent model for the study of esophageal carcinogenesis (https://sciencellonline.com/human-esophageal-epithelial-cells).

To rule out the possibility that Cr(VI) itself directly enhances the malignant proliferation, we treated HEECs with 0.25 μmol/L of Cr(VI) for 48 h. The soft agar colony formation assay revealed that HEECs with acute exposure to Cr(VI) failed to develop colonies in soft agar. Additionally, CCK-8, EdU incorporation, sphere formation, and transwell assays demonstrated that acute exposure to Cr(VI) had no effects on HEEC proliferation, stemness, or motility. These results further confirmed that it is Cr(VI)-induced transformation, not Cr(VI) itself, that confers the property of malignant proliferation to HEECs. Interestingly, Sheng et al. (2021) found that 24 and 48 h of exposure to Cr(VI) (0.4 μmol/L) promoted the proliferation, migration, and invasion of bladder cancer cells by regulating Filamin A (*FLNA*). Another study from the same research team revealed that acute exposure to Cr(VI) enhanced the migration of prostate cancer cells by promoting EMT (Zhang et al., 2019). Taken together, these findings indicate that the impacts of short-term exposure to Cr(VI) on proliferation and EMT are different between normal epithelial cells and cancer cells.

In an attempt to clarify the mechanism by which Cr(VI) induced malignant proliferation of HEECs, RNA-Seq analysis was performed in HEECs and HEEC-Cr(VI) cells to obtain the profile of DEGs. Further exploration based on GSEA identified abnormal activation of the Notch signaling pathway. Notch signaling is an evolutionarily conserved pathway that is closely associated with the development process, physiological homeostasis, and tissue renewal (Zhou et al., 2022). It has been reported that Notch signaling regulates the development of the esophageal squamous epithelium in the normal esophagus and acts as a tumor suppressor pathway to inhibit esophagus tumorigenesis induced by 4-nitroquinoline 1-oxide (Sawangarun et al., 2018). However, the dysregulation of the Notch signaling functions with a dual role, an oncogenic or a tumor-suppressor pathway, in esophagus carcinogenesis, which is totally dependent on the specific cellular and genetic context (Ranganathan et al., 2011; Sun et al., 2014; Zhong et al., 2015; Nowell and Radtke, 2017; Li Y et al., 2021). In the present study, to confirm the function of abnormally activated Notch signaling in the malignant proliferation of HEEC-Cr(VI), we performed the blocking experiments by applying DAPT, an inhibitor against the Notch signaling pathway, and determined its essential role in maintaining a tumor-like proliferative capacity. Remarkably, Natsuizaka et al. (2017) reported that activated Notch signaling in ESCC accelerates EMT and tumor initiation via increasing cancer stem cells, while our study found that the activation of the Notch pathway and enhanced stemness in HEEC-Cr(VI) cells were accompanied by increased E-cadherin expression. Additionally, DAPT treatment failed to affect E-cadherin and MMP-2 expression in HEEC-Cr(VI) cells, suggesting that Notch signaling is not involved in regulating EMT during Cr(VI)-induced malignant transformation of HEECs. Interestingly, hypoxia-induced ROS was demonstrated to accelerate the migration, invasion, and EMT of glioblastoma cells via activating the hypoxia-inducible factor-1α (HIF-1α) signaling (Zhang et al., 2023). The potential interaction between hypoxia or ROS and chronic exposure to Cr(VI) might be worth further exploring.

According to the guideline value from the World Health Organization (WHO, 2022), total chromium in drinking water should not exceed 50 μg/L. Some regions have set stricter restrictions for Cr(VI) in drinking water, such as a limit of 10 μg/L in California or 5 μg/L in Italy (Chrysochoou et al., 2016). However, the Cr(VI) concentration in the groundwater of some regions with ultramafic rocks has been reported to be

between 0.2 and 180 μg/L (Chrysochoou et al., 2016). For example, in La Spezia (Italy), the concentration of Cr(VI) in the groundwater reached 73 μg/L, significantly exceeding the limitation of 5 μg/L (Fantoni et al., 2002). In our study, the applied concentration of K_2CrO_4 is 0.25 μmol/L, equivalent to 13 μg/L of total chromium, which is lower than the guideline value from WHO and the Cr(VI) concentration in groundwater of some ultramafic regions. It is worth noting that one study focusing on arsenic and chromium topsoil levels revealed an association between chromium concentration in topsoil and women's EC mortality in Spain (Núñez et al., 2016). Furthermore, a case-control study by Nozadi et al. (2021) reported that chromium concentrations ((8.10±7.31) μg/kg) of EC from Eastern Iraq, an area with heavy metal pollution, displayed a notable rise compared to non-cancerous tissues ((1.98±0.80) μg/kg). If assuming tissue density to be approximately 1 kg/dm^3, the concentration ((8.10±7.31) μg/kg) could be considered, which is very close to the exposure dose of Cr(VI) (0.25 μmol/L or 13 μg/L) used in our study. Given that we have demonstrated the capacity of chronic Cr(VI) (0.25 μmol/L) exposure to induce malignant transformation of HEECs, this study provides a crucial reference for future exploration related to cancer initiation or public health, which will raise more and broader attention to chromium contamination.

5 Conclusions

As a summary, we demonstrated the driving role of chronic exposure to Cr(VI) in esophagus tumorigenesis and clarified the relevant mechanism by which Cr(VI)-induced activation of the Notch signaling contributes to the malignant proliferation and stemness of HEEC-Cr(VI) cells. Our study provides a novel potential target for clinical therapy of Cr(VI)-related esophageal tumors.

Data availability statement

All data about this study are present in the article and/or supplementary data.

Acknowledgments

This work was supported by the Special Construction Project Fund for Taishan Mountain Scholars of Shandong Province, the Jinan Medicine Research Program, the Nurturing and Development Fund from The Second Hospital of Shandong University (No. 2022YP62), and the Shandong Provincial Natural Science Foundation for Young Scholars (No. ZR2022QH285), China.

Author contributions

Peichao LI and Xiaogang ZHAO contributed to the conception and design of this project. Yilin ZHU performed most of the experiments and data analysis. Fanrong LIU, Lei LIU, Jinfu WANG, and Fengyuan GAO assisted with bench work. Lan YE, Honglei WU, and Chengjun ZHOU provided technical assistance for animal experiments. Peichao LI and Yilin ZHU wrote this manuscript. Guimei LIN and Xiaogang ZHAO revised this manuscript. Peichao LI supervised the processes of this project. All authors have reviewed and approved the final manuscript, and therefore, have full access to all the data in the study and take responsibility for the integrity and security of the data.

Compliance with ethics guidelines

Yilin ZHU, Fanrong LIU, Lei LIU, Jinfu WANG, Fengyuan GAO, Lan YE, Honglei WU, Chengjun ZHOU, Guimei LIN, Xiaogang ZHAO, and Peichao LI declare that they have no conflict of interest.

All experiments involved in mice were conducted in the Animal Research Center of The Second Hospital of Shandong University and approved by the Ethical Committee for Animal Experimentation of The Second Hospital of Shandong University (No. KYLL-2022A195).

References

Abnet CC, Arnold M, Wei WQ, 2018. Epidemiology of esophageal squamous cell carcinoma. *Gastroenterology*, 154(2):360-373. https://doi.org/10.1053/j.gastro.2017.08.023

Amer MH, El-Yazigi A, Hannan MA, et al., 1990. Water contamination and esophageal cancer at Gassim Region, Saudi Arabia. *Gastroenterology*, 98(5):1141-1147. https://doi.org/10.1016/0016-5085(90)90326-v

An L, Zheng RS, Zeng HM, et al., 2023. The survival of esophageal cancer by subtype in China with comparison to the United States. *Int J Cancer*, 152(2):151-161. https://doi.org/10.1002/ijc.34232

Aponte PM, Caicedo A, 2017. Stemness in cancer: stem cells, cancer stem cells, and their microenvironment. *Stem Cells Int*, 2017:5619472. https://doi.org/10.1155/2017/5619472

Brabletz S, Schuhwerk H, Brabletz T, et al., 2021. Dynamic EMT: a multi-tool for tumor progression. *EMBO J*, 40(18): e108647. https://doi.org/10.15252/embj.2021108647

Cai JY, Qiao YJ, Chen LB, et al., 2024. Regulation of the Notch signaling pathway by natural products for cancer therapy. *J Nutr Biochem*, 123:109483.

https://doi.org/10.1016/j.jnutbio.2023.109483

Chen QY, Murphy A, Sun H, et al., 2019. Molecular and epigenetic mechanisms of Cr(VI)-induced carcinogenesis. *Toxicol Appl Pharmacol*, 377:114636. https://doi.org/10.1016/j.taap.2019.114636

Chrysochoou M, Theologou E, Bompoti N, et al., 2016. Occurrence, origin and transformation processes of geogenic chromium in soils and sediments. *Curr Pollution Rep*, 2(4): 224-235. https://doi.org/10.1007/s40726-016-0044-2

Fantoni D, Brozzo G, Canepa M, et al., 2002. Natural hexavalent chromium in groundwaters interacting with ophiolitic rocks. *Environ Geol*, 42(8):871-882. https://doi.org/10.1007/s00254-002-0605-0

Freedman VH, Shin SI, 1974. Cellular tumorigenicity in *nude* mice: correlation with cell growth in semi-solid medium. *Cell*, 3(4):355-359. https://doi.org/10.1016/0092-8674(74)90050-6

Goldman MJ, Craft B, Hastie M, et al., 2020. Visualizing and interpreting cancer genomics data via the Xena platform. *Nat Biotechnol*, 38(6):675-678. https://doi.org/10.1038/s41587-020-0546-8

Hashemian M, Murphy G, Etemadi A, et al., 2017. Toenail mineral concentration and risk of esophageal squamous cell carcinoma, results from the Golestan Cohort Study. *Cancer Med*, 6(12):3052-3059. https://doi.org/10.1002/cam4.1247

Hsieh MH, Choe JH, Gadhvi J, et al., 2019. P63 and SOX2 dictate glucose reliance and metabolic vulnerabilities in squamous cell carcinomas. *Cell Rep*, 28(7):1860-1878.e9. https://doi.org/10.1016/j.celrep.2019.07.027

Hu GP, Li P, Li Y, et al., 2016. Methylation levels of P16 and TP53 that are involved in DNA strand breakage of 16HBE cells treated by hexavalent chromium. *Toxicol Lett*, 249: 15-21. https://doi.org/10.1016/j.toxlet.2016.03.003

Hu GP, Li P, Cui XX, et al., 2018. Cr(VI)-induced methylation and down-regulation of DNA repair genes and its association with markers of genetic damage in workers and 16HBE cells. *Environ Pollut*, 238:833-843. https://doi.org/10.1016/j.envpol.2018.03.046

Islam S, Kamila S, Chattopadhyay A, 2022. Toxic and carcinogenic effects of hexavalent chromium in mammalian cells *in vivo* and *in vitro*: a recent update. *J Environ Sci Health Part C*, 40(3-4):282-315. https://doi.org/10.1080/26896583.2022.2158675

Iyer M, Anand U, Thiruvenkataswamy S, et al., 2023. A review of chromium (Cr) epigenetic toxicity and health hazards. *Sci Total Environ*, 882:163483. https://doi.org/10.1016/j.scitotenv.2023.163483

Jiang AL, Gong LJ, Ding H, et al., 2021. Cancer mortality and long-term environmental exposure of cadmium in contaminated community based on a third retrospective cause of death investigation of residents living in the Guangdong Province from 2004 to 2005. *Biol Trace Elem Res*, 199(12): 4504-4515. https://doi.org/10.1007/s12011-021-02599-0

Jing N, Gao WQ, Fang YX, 2021. Regulation of formation, stemness and therapeutic resistance of cancer stem cells. *Front Cell Dev Biol*, 9:641498. https://doi.org/10.3389/fcell.2021.641498

Kopan R, Ilagan MXG, 2009. The canonical Notch signaling pathway: unfolding the activation mechanism. *Cell*, 137(2): 216-233. https://doi.org/10.1016/j.cell.2009.03.045

Lee CP, Lee YH, Lian IB, et al., 2016. Increased prevalence of esophageal cancer in areas with high levels of nickel in farm soils. *J Cancer*, 7(12):1724-1730. https://doi.org/10.7150/jca.15441

Li PC, Zhang XR, Murphy AJ, et al., 2021. Downregulation of hedgehog-interacting protein (HHIP) contributes to hexavalent chromium-induced malignant transformation of human bronchial epithelial cells. *Carcinogenesis*, 42(1): 136-147. https://doi.org/10.1093/carcin/bgaa085

Li XX, Yan XC, Wang YF, et al., 2023. The Notch signaling pathway: a potential target for cancer immunotherapy. *J Hematol Oncol*, 16:45. https://doi.org/10.1186/s13045-023-01439-z

Li Y, Li YH, Chen XX, 2021. NOTCH and esophageal squamous cell carcinoma. *In*: Reichrath J, Reichrath S (Eds.), Notch Signaling in Embryology and Cancer: Notch Signaling in Cancer. Springer, Cham, p.59-68. https://doi.org/10.1007/978-3-030-55031-8_5

Love MI, Huber W, Anders S, 2014. Moderated estimation of fold change and dispersion for RNA-seq data with DESeq2. *Genome Biol*, 15:550. https://doi.org/10.1186/s13059-014-0550-8

Morgan E, Soerjomataram I, Rumgay H, et al., 2022. The global landscape of esophageal squamous cell carcinoma and esophageal adenocarcinoma incidence and mortality in 2020 and projections to 2040: new estimates from GLOBOCAN 2020. *Gastroenterology*, 163(3):649-658.e2. https://doi.org/10.1053/j.gastro.2022.05.054

National Toxicology Program, 2008. Toxicology and Carcinogenesis Studies of Sodium Dichromate Dihydrate (CAS No. 7789-12-0) in F344/N rats and B6C3F1 mice (drinking water studies). NTP TR 546, National Toxicology Program, Research Triangle Park, NC.

Natsuizaka M, Whelan KA, Kagawa S, et al., 2017. Interplay between Notch1 and Notch3 promotes EMT and tumor initiation in squamous cell carcinoma. *Nat Commun*, 8:1758. https://doi.org/10.1038/s41467-017-01500-9

Nowell CS, Radtke F, 2017. Notch as a tumour suppressor. *Nat Rev Cancer*, 17(3):145-159. https://doi.org/10.1038/nrc.2016.145

Nozadi F, Azadi N, Mansouri B, et al., 2021. Association between trace element concentrations in cancerous and noncancerous tissues with the risk of gastrointestinal cancers in Eastern Iran. *Environ Sci Pollut Res Int*, 28(44):

62530-62540.
https://doi.org/10.1007/s11356-021-15224-3

Núñez O, Fernández-Navarro P, Martín-Méndez I, et al., 2016. Arsenic and chromium topsoil levels and cancer mortality in Spain. *Environ Sci Pollut Res Int*, 23(17):17664-17675.
https://doi.org/10.1007/s11356-016-6806-y

Ranganathan P, Weaver KL, Capobianco AJ, 2011. Notch signalling in solid tumours: a little bit of everything but not all the time. *Nat Rev Cancer*, 11(5):338-351.
https://doi.org/10.1038/nrc3035

Sawangarun W, Mandasari M, Aida J, et al., 2018. Loss of Notch1 predisposes oro-esophageal epithelium to tumorigenesis. *Exp Cell Res*, 372(2):129-140.
https://doi.org/10.1016/j.yexcr.2018.09.019

Schneider CA, Rasband WS, Eliceiri KW, 2012. NIH Image to ImageJ: 25 years of image analysis. *Nat Methods*, 9(7):671-675.
https://doi.org/10.1038/nmeth.2089

Sheng F, Chen KX, Liu J, et al., 2021. Chromium (VI) promotes EMT by regulating FLNA in BLCA. *Environ Toxicol*, 36(8):1694-1701.
https://doi.org/10.1002/tox.23165

Shin SI, Freedman VH, Risser R, et al., 1975. Tumorigenicity of virus-transformed cells in *nude* mice is correlated specifically with anchorage independent growth *in vitro*. *Proc Natl Acad Sci USA*, 72(11):4435-4439.
https://doi.org/10.1073/pnas.72.11.4435

Sohrabi M, Nikkhah M, Sohrabi M, et al., 2021. Evaluating tissue levels of the eight trace elements and heavy metals among esophagus and gastric cancer patients: a comparison between cancerous and non-cancerous tissues. *J Trace Elem Med Biol*, 68:126761.
https://doi.org/10.1016/j.jtemb.2021.126761

Stout MD, Herbert RA, Kissling GE, et al., 2009. Hexavalent chromium is carcinogenic to F344/N rats and B6C3F1 mice after chronic oral exposure. *Environ Health Perspect*, 117(5):716-722.
https://doi.org/10.1289/ehp.0800208

Subramanian A, Tamayo P, Mootha VK, et al., 2005. Gene set enrichment analysis: a knowledge-based approach for interpreting genome-wide expression profiles. *Proc Natl Acad Sci USA*, 102(43):15545-15550.
https://doi.org/10.1073/pnas.0506580102

Sun H, Clancy HA, Kluz T, et al., 2011. Comparison of gene expression profiles in chromate transformed BEAS-2B cells. *PLoS ONE*, 6(3):e17982.
https://doi.org/10.1371/journal.pone.0017982

Sun H, Brocato J, Costa M, 2015. Oral chromium exposure and toxicity. *Curr Environ Health Rep*, 2(3):295-303.
https://doi.org/10.1007/s40572-015-0054-z

Sun WY, Gaykalova DA, Ochs MF, et al., 2014. Activation of the *NOTCH* pathway in head and neck cancer. *Cancer Res*, 74(4):1091-1104.
https://doi.org/10.1158/0008-5472.CAN-13-1259

Sung H, Ferlay J, Siegel RL, et al., 2021. Global cancer statistics 2020: GLOBOCAN estimates of incidence and mortality worldwide for 36 cancers in 185 countries. *CA Cancer J Clin*, 71(3):209-249.
https://doi.org/10.3322/caac.21660

Tang DD, Chen MJ, Huang XH, et al., 2023. SRplot: a free online platform for data visualization and graphing. *PLoS ONE*, 18(11):e0294236.
https://doi.org/10.1371/journal.pone.0294236

WHO (World Health Organization), 2022. Guidelines for Drinking-Water Quality: Fourth Edition Incorporating the First and Second Addenda. World Health Organization, Geneva, Switzerland. https://www.who.int/publications/i/item/9789240045064

You BH, Yoon JH, Kang H, et al., 2019. HERES, a lncRNA that regulates canonical and noncanonical Wnt signaling pathways via interaction with EZH2. *Proc Natl Acad Sci USA*, 116(49):24620-24629.
https://doi.org/10.1073/pnas.1912126116

Zeidler-Erdely PC, Falcone LM, Antonini JM, et al., 2020. Tumorigenic response in lung tumor susceptible A/J mice after sub-chronic exposure to calcium chromate or iron (III) oxide. *Toxicol Lett*, 334:60-65.
https://doi.org/10.1016/j.toxlet.2020.09.012

Zhang CW, Cai KK, Feng QJ, et al., 2019. Chromium(VI) promotes cell migration through targeting epithelial-mesenchymal transition in prostate cancer. *Toxicol Lett*, 300:10-17.
https://doi.org/10.1016/j.toxlet.2018.10.012

Zhang L, Cao YY, Guo XX, et al., 2023. Hypoxia-induced ROS aggravate tumor progression through HIF-1α-SERPINE1 signaling in glioblastoma. *J Zhejiang Univ-Sci B (Biomed & Biotechnol)*, 24(1):32-49.
https://doi.org/10.1631/jzus.B2200269

Zhang ZC, Cao HY, Song N, et al., 2020. Long-term hexavalent chromium exposure facilitates colorectal cancer in mice associated with changes in gut microbiota composition. *Food Chem Toxicol*, 138:111237.
https://doi.org/10.1016/j.fct.2020.111237

Zhong R, Bao RY, Faber PW, et al., 2015. Notch1 activation or loss promotes HPV-induced oral tumorigenesis. *Cancer Res*, 75(18):3958-3969.
https://doi.org/10.1158/0008-5472.CAN-15-0199

Zhou BH, Lin WL, Long YL, et al., 2022. Notch signaling pathway: architecture, disease, and therapeutics. *Signal Transduct Target Ther*, 7:95.
https://doi.org/10.1038/s41392-022-00934-y

Supplementary information

Tables S1 and S2; Figs. S1–S9; Raw data for western blot